International Journal of Control, Automation, and Systems 22(4) (2024) 1360-1370
http://dx.doi.org/10.1007/s12555-022-0601-y
ISSN:1598-6446 eISSN:2005-4092
http://www.springer.com/12555

# Variable Impedance Control for a Single Leg of a Quadruped Robot Based on Contact Force Estimation

**Yanan Fan*, Zhongcai Pei, and Zhiyong Tang**

**Abstract:** A quadruped robot interacts with the ground during the stance phase. This interaction will have a great impact on the feet, torso and joints of the robot, thus affecting the stability of its movement and reducing its adaptability in complex environments with features such as uneven terrain. The contact between each foot of the quadruped robot and the ground should not only control the movement trajectory of the leg but also control the force between the leg and the ground to comply with the environmental constraints. In general, the environment is constantly changing, whereas the traditional impedance control parameters are fixed and thus impose fixed-point constraints. To improve the compliance of the feet of a robot and achieve flexible interactions with the ground in various complex environments, such as pipelines, ruins and forests, variable impedance control is proposed. Based on variable inertia, damping and stiffness parameters, a new Lyapunov function is selected to analyse the stability of the closed-loop system. Furthermore, a force estimator is applied to estimate the contact forces, thereby reducing the burden of structural design and the cost of the robot. The effectiveness of the proposed variable impedance control scheme and contact force estimator is verified through numerical simulations in MATLAB.

**Keywords:** Dynamics, force estimation, quadruped robot, variable impedance control.

## 1. INTRODUCTION

Legged robots have attracted extensive attention in recent years due to their strong environmental adaptability, high flexibility and fast movement speed. Legged robots can be divided into two legs, four legs, six legs and eight legs. In particular, quadruped bionic robots have become key research objects because of their superior field walking ability and load capacity [1]. At present, quadruped robots have been applied in material transportation [2,3], emergency rescue [4], home services [5,6], military surveys [7], and engineering exploration [8], among other fields. Most quadruped robots have rigid structures composed of a series of rigid links, prismatic pairs and revolute pairs. Consequently, large rigid collisions will occur between the robot and the ground. This can cause such a robot to be prone to vibrations, which may even result in loss of stability. Therefore, a simple position control strategy cannot satisfy the design needs of a corresponding controller. As an alternative, a flexible force control strategy requires an accurate dynamics model, which increases the difficulty of robot control [9]. Therefore, hybrid force/position control and impedance control are two commonly used approaches in the field of robotics. Compliance control can achieve the desired motion while also ensuring that a robot can interact with its environment in a friendly manner. In hybrid force/position control, the task space is decoupled into a position subspace and force subspace; accordingly, position control and force control are carried out separately in these two subspaces, ignoring the dynamic coupling between the robot and the environment [10]. Hogan [11] proposed the impedance control approach by establishing the dynamic relationship between the motion of the robot and the external force acting on it, thereby providing a unified framework for the position control of the robot in free space and the compliance control of environment interactions.

In view of the advantages of impedance control, reference [12] applied impedance control in a quadruped robot to compensate for the influence of the weight of the legs on the centre of gravity of the robot to achieve walking stability. Considering the compliance of the end effector of a surgical robot, Xiao *et al*. [13] investigated the impedance control of a minimally invasive surgical robot and determined the impedance control parameters in accordance with collected data so as to avoid excessive insertion force between the robot end effector and human tissue. The impedance control strategy has been widely employed in exoskeleton robots for rehabilitation [14] because impedance control can not only control the posi-

Manuscript received June 30, 2022; revised November 2, 2022, January 30, 2023, and April 28, 2023; accepted May 10, 2023. Recommended by Senior Editor Kyoung Kwan Ahn.

Yanan Fan, Zhongcai Pei, and Zhiyong Tang are with the School of Automation Science and Electrical Engineering, Beihang University, Beijing 100191, China (e-mails: 535424873@qq.com, {peizc, zyt_76}@buaa.edu.cn).
* Corresponding author.

tion of a robot but also maintain the human-robot interaction force in a safe range, allowing the patient to perform rehabilitation training in accordance with predetermined movements [15]. Ochoa *et al*. [16] realized a mould polishing operation for a 7 degree of freedom (DOF) robot within the impedance control framework. Notably, the previous research work on impedance control has mainly focused on constant impedance control; that is, the inertia parameters, damping parameters and stiffness parameters have been expressed as constant matrices. In practical applications, however, the typical working environment of a robot is relatively complex. For example, when a quadruped robot walks on a rough road with inconsistent stiffness, it will be difficult to achieve good walking performance if the impedance control parameters remain unchanged. Therefore, constant impedance control cannot guarantee the motion accuracy of a robot or the dynamic performance of its control system. Accordingly, in recent years, some scholars have begun to explore the potential of variable impedance control for improving the flexibility and safety of robot operations. Lee *et al*. [17] defined the stiffness parameters as a time-varying matrix to track the contact forces of a 7-DOF manipulator platform. Reference [18] proposed an impedance control scheme with time-varying damping and stiffness parameters based on the pin insertion task on the KUKA iiwa collaborative robot test platform. In [19], variable impedance control was applied for apple picking. To reduce the damage caused to the apples during the picking process, three self-tuning control parameters were defined to enhance the performance of the force-based impedance control system.

Although variable impedance control improves the dexterity and dynamic performance of the controlled system [20], its control parameters make the traditional system stability analysis method no longer applicable and increase the difficulty of performance analysis for the controlled system. In [21], a 7-DOF manipulator was used to simulate a surgical suturing process. Time-varying stiffness parameters can allow the impedance characteristics to be adjusted in accordance with the unique properties of different people and different tissue layers. However, such time-varying stiffness parameters will also inject additional energy into the system and make the system unstable. To allow a manipulator to stably interact with its external environment, the concept of a virtual energy tank has been introduced to store the energy dissipated by the controlled system in order to adjust the time-varying stiffness so as to ensure the stability of the system [22]. Unfortunately, this method depends on the initial state of the system. Park *et al*. [23] proposed an input-state-stable variable impedance controller for a manipulator by defining a Lyapunov function that includes both the kinetic energy and potential energy and designing a variable stiffness update law to ensure the asymptotic stability of the system. Kronander *et al*. [24] proposed state-independent stability conditions for time-varying stiffness and damping matrices by referring to the method of adaptive selection of the energy function, namely, a weighted quadratic energy function that includes both the velocity error and position error. Variable impedance control can simultaneously adjust the dynamic relationship between the motion and contact force of a robot and flexibly adjust the dynamic characteristics of the system in accordance with environmental changes that occur during the execution of interactive tasks [25]. Recently, variable impedance control has attracted the attention of many scholars; however, there has been little related academic literature in the field of quadruped robots to date. Reference [26] studied constant impedance control for a quadruped robot. This method does not allow for dynamic changes in the operating stiffness of the foot, although variable stiffness is quite significant for enabling dynamic interaction between a quadruped robot and its environment, which is beneficial for helping the robot to walk smoothly. The ability to perceive force is essential for adapting to an unknown environment and achieving compliance control of a robot [27]. The traditional method is to install force sensors on the robot. However, the installation of force sensors will impose a burden on the overall structure of the robot, raise the complexity of system operation and increase the cost of the system. As an alternative, designing a force estimator for a robot rather than directly equipping it with sensors can reduce the design difficulty, and enable the robot to sense collisions, external interference, environmental changes, etc. [28].

In this paper, a variable impedance control scheme for a single leg of a quadruped robot is primarily studied. The main contributions are as follows:

1) To endow the quadruped robot with a force sensing ability while avoiding complex structural components such as force sensors, a contact force estimator is designed based on a nonlinear disturbance observer for the single-leg workspace. Moreover, the convergence of the contact force tracking error is proven.
2) To ensure the contact flexibility of the quadruped robot and enable the robot to independently adjust its control parameters when moving on complex and uneven terrain, a variable impedance controller based on the operation space is proposed for a single-leg model of the quadruped robot, in which the time-varying impedance control parameters include a time-varying inertia matrix, a time-varying damping matrix and a time-varying stiffness matrix.
3) Because the control parameters are varying in time, the traditional Lyapunov function selection method will continuously inject potential energy into the system. In this paper, a new Lyapunov structure including time-varying impedance control parameters is adopted to analyse the stability of the system, and

state-independent constraint conditions are proposed to ensure system stability.

4) The proposed variable impedance controller is implemented in the operation space, thus allowing the quadruped robot to perform the desired task by means of coupled force-position constraints and avoiding the occurrence of an acceleration term.

The structure of this paper is as follows: In Section 2, the dynamics modelling for a single leg of a quadruped robot is briefly introduced. In Section 3, a force estimator is designed. Section 4 introduces the implementation of the proposed variable impedance controller in the operation space. In Section 5, MATLAB numerical simulations are presented to verify the feasibility of the proposed variable impedance control method and force estimator. Finally, in Section 6, the conclusion is given.

## 2. DYNAMICS MODELLING FOR A SINGLE LEG OF A QUADRUPED ROBOT

In this paper, a single leg of a quadruped robot is taken as the research object. The single-leg structure model of the quadruped robot is shown in Fig. 1. Each leg has 3 degrees of freedom and is composed of three connecting rods connected through revolute pairs.

To model a single leg of the robot, the single-leg structure model is simplified as shown in Fig. 2, where $x_H$-$y_H$-$z_H$ is the base frame of the leg; $x_i$-$y_i$-$z_i$ for $i$ = 1, 2, 3 and 4 are the coordinate frames of the rolling hip joint, pitching hip joint, knee joint and foot, respectively; and $l_1$, $l_2$ and $l_3$ are the rod lengths.

In this paper, the dynamics model of a single leg mechanism is established based on the Lagrange function [29], which is an effective and widely used method. By applying the Euler-Lagrange equation [30], the dynamics of a single leg mechanism can be described in the following normal form

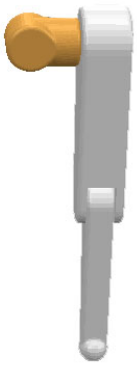

Fig. 1. The single-leg structure of the quadruped robot.

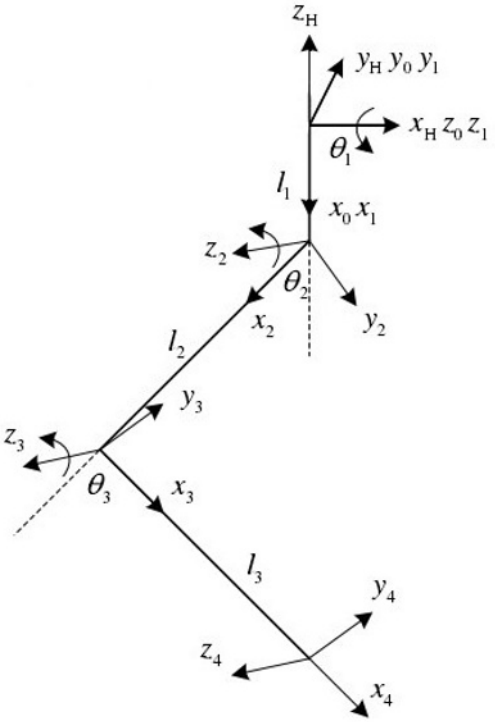


Fig. 2. Schematic diagram of the single-leg structure.

$$\boldsymbol{M}\ddot{\boldsymbol{\theta}} + \Gamma \begin{bmatrix} \dot{\theta}_1\dot{\theta}_1 \\ \dot{\theta}_2\dot{\theta}_2 \\ \dot{\theta}_3\dot{\theta}_3 \\ \dot{\theta}_1\dot{\theta}_2 \\ \dot{\theta}_1\dot{\theta}_3 \\ \dot{\theta}_2\dot{\theta}_3 \end{bmatrix} + \boldsymbol{G} = \boldsymbol{\tau}. \tag{1}$$

In (1), $\boldsymbol{M} \in \Re^{3\times3}$ is the inertia matrix, $\Gamma \in \Re^{3\times6}$, $\boldsymbol{G} \in \Re^{3\times1}$ is the gravity term, $\boldsymbol{\tau} \in \Re^{3\times1}$ is the actuation torque, and $\ddot{\boldsymbol{\theta}} = \begin{bmatrix} \ddot{\theta}_1 & \ddot{\theta}_2 & \ddot{\theta}_3 \end{bmatrix}^{\mathrm{T}}$ is the angular acceleration. $\boldsymbol{\Gamma} \begin{bmatrix} \dot{\theta}_1\dot{\theta}_1 \\ \dot{\theta}_2\dot{\theta}_2 \\ \dot{\theta}_3\dot{\theta}_3 \\ \dot{\theta}_1\dot{\theta}_2 \\ \dot{\theta}_1\dot{\theta}_3 \\ \dot{\theta}_2\dot{\theta}_3 \end{bmatrix}$ is the Coriolis force and centrifugal force term, in accordance with the properties of the robot dynamics model [29]

$$\boldsymbol{\Gamma} = \frac{\partial M_{ij}}{\partial \theta_k} - 0.5\frac{\partial M_{jk}}{\partial \theta_i},\ (i,\ j,\ k = 1,\ 2,\ 3). \tag{2}$$

The Coriolis force and centrifugal force term can be further simplified as

$$\boldsymbol{C}(\theta, \dot{\theta}) = \boldsymbol{\Gamma}\dot{\boldsymbol{\theta}}. \tag{3}$$

Then, the dynamics model based on the configuration space can be rewritten as

$$\boldsymbol{M}\ddot{\boldsymbol{\theta}} + \boldsymbol{C}(\boldsymbol{\theta}, \dot{\boldsymbol{\theta}})\dot{\boldsymbol{\theta}} + \boldsymbol{G} = \boldsymbol{\tau}. \tag{4}$$

Usually, the desired trajectory of the robot is planned in the operation space. Thus, to facilitate the compliance control of the robot in the standing phase, the dynamics model in the configuration space should be further translated into the operation space. By defining $\boldsymbol{q}_e = \begin{bmatrix} x \\ y \\ z \end{bmatrix}$ as the trajectory of the foot, the differential of $q_e$ with respect to time can be derived as follows:

$$\dot{\boldsymbol{q}}_e = \boldsymbol{J}\dot{\boldsymbol{\theta}}. \tag{5}$$

$\boldsymbol{J} \in \Re^{3\times 3}$ represents the Jacobian matrix for the transformation from the configuration space to the operation space. Taking the derivative of (5) results in

$$\ddot{\boldsymbol{q}}_e = \boldsymbol{J}\ddot{\boldsymbol{\theta}} + \dot{\boldsymbol{J}}\dot{\boldsymbol{\theta}}. \tag{6}$$

Now, by multiplying both sides of (4) by $\boldsymbol{J}^{-\mathrm{T}}$ and substituting (5) and (6) into (4), the dynamics equation of the leg can be rewritten in the following compact form

$$\boldsymbol{M}_e\ddot{\boldsymbol{q}}_e + \boldsymbol{C}_e\dot{\boldsymbol{q}}_e + \boldsymbol{G}_e = \boldsymbol{\tau}_e. \tag{7}$$

In (7), $\boldsymbol{M}_e = \boldsymbol{J}^{-\mathrm{T}}\boldsymbol{M}\boldsymbol{J}^{-1}$ denotes the inertia matrix in the operation space, $\boldsymbol{C}_e = J^{-\mathrm{T}}(\boldsymbol{C} - \boldsymbol{M}\boldsymbol{J}^{-1}\dot{\boldsymbol{J}}\boldsymbol{J}^{-1})$ represents the Coriolis force and centrifugal force matrix in the operation space, $\boldsymbol{G}_e = \boldsymbol{J}^{-\mathrm{T}}\boldsymbol{G}$ is the gravitational force vector in the operation space, and $\boldsymbol{\tau}_e = \boldsymbol{J}^{-\mathrm{T}}\boldsymbol{\tau}$ is the actuation torque in the operation space.

In the stance phase, considering the contact force, the dynamics model of (7) becomes [31]

$$\boldsymbol{M}_e\ddot{\boldsymbol{q}}_e + \boldsymbol{C}_e\dot{\boldsymbol{q}}_e + \boldsymbol{G}_e = \boldsymbol{\tau}_e + \boldsymbol{\tau}_{out}, \tag{8}$$

where $\boldsymbol{\tau}_{out}$ is the contact force. A quadruped robot is a relatively complex system. However, the installation of a force sensor to sense the external contact force has several disadvantages, such as increasing the costs of implementation and maintenance of the robot. Instead of relying on a force sensor, designing a force estimator to indirectly sense the external contact force is an economical and effective alternative.

## 3. FORCE ESTIMATOR DESIGN

### 3.1. Force estimator design

Sensorless technology provides an alternative means of determining contact forces [32]. Previous research on external force estimators has been based on Newton's law [33] and disturbance estimation [34], among other approaches. These force estimation models usually include an acceleration parameter, although a recently proposed method based on generalized momentum overcomes the problems presented by the acceleration term and the impact of system noise [35]. However, the accuracy with which the contact force can be estimated based on the generalized momentum is dependent on the gain parameters, and the stability of such estimators has rarely been proven in the literature. In this paper, the foot contact force in the closed-loop system is estimated based on a nonlinear disturbance observer [28].

For estimating the contact force $\boldsymbol{\tau}_{out}$, according to the dynamic system given in (8), the auxiliary variable $\boldsymbol{z}$ is defined as

$$\boldsymbol{z} = \hat{\boldsymbol{\tau}}_{out} - \boldsymbol{p}(\boldsymbol{q}_e, \dot{\boldsymbol{q}}_e), \tag{9}$$

where the vector $\boldsymbol{p}(\boldsymbol{q}_e, \dot{\boldsymbol{q}}_e)$ can be obtained from the nonlinear estimator gain matrix $\boldsymbol{L}(\boldsymbol{q}_e, \dot{\boldsymbol{q}}_e)$

$$\frac{d}{dt}\boldsymbol{p}(\boldsymbol{q}_e, \dot{\boldsymbol{q}}_e) = \boldsymbol{L}(\boldsymbol{q}_e, \dot{\boldsymbol{q}}_e)\boldsymbol{M}_e\ddot{\boldsymbol{q}}_e. \tag{10}$$

In (10), the gain matrix $\boldsymbol{L}(\boldsymbol{q}_e, \dot{\boldsymbol{q}}_e)$ can be expressed as

$$\boldsymbol{L}(\boldsymbol{q}_e, \dot{\boldsymbol{q}}_e) = X^{-1}\boldsymbol{M}_e^{-1}, \tag{11}$$

where $X$ is a constant matrix; then, $\boldsymbol{p}$ can be derived as

$$\boldsymbol{p} = X^{-1}\dot{\boldsymbol{q}}_e. \tag{12}$$

Taking the derivative of (9), we obtain

$$\begin{aligned} \dot{\boldsymbol{z}} &= \dot{\hat{\boldsymbol{\tau}}}_{out} - \dot{\boldsymbol{p}}(\boldsymbol{q}_e, \dot{\boldsymbol{q}}_e) \\ &= \dot{\hat{\boldsymbol{\tau}}}_{out} - \boldsymbol{L}(\boldsymbol{q}_e, \dot{\boldsymbol{q}}_e)\boldsymbol{M}_e\ddot{\boldsymbol{q}}_e, \end{aligned} \tag{13}$$

where $\dot{\hat{\boldsymbol{\tau}}}_{out}$ is defined as

$$\dot{\hat{\boldsymbol{\tau}}}_{out} = -\boldsymbol{L}\hat{\boldsymbol{\tau}}_{out} + \boldsymbol{L}(\boldsymbol{M}_e\ddot{\boldsymbol{q}}_e + \boldsymbol{C}_e\dot{\boldsymbol{q}}_e + \boldsymbol{G}_e - \boldsymbol{\tau}_e). \tag{14}$$

Substituting (8), (9) and (14) into (13) yields

$$\begin{aligned} \dot{\boldsymbol{z}} = &-\boldsymbol{L}(\boldsymbol{q}_e, \dot{\boldsymbol{q}}_e)\boldsymbol{z} \\ &+\boldsymbol{L}(\boldsymbol{q}_e, \dot{\boldsymbol{q}}_e)(\boldsymbol{C}_e\dot{\boldsymbol{q}}_e + \boldsymbol{G}_e - \boldsymbol{\tau}_e - \boldsymbol{p}(\boldsymbol{q}_e, \dot{\boldsymbol{q}}_e)). \end{aligned} \tag{15}$$

Then, according to (12) and (15), the contact force $\boldsymbol{\tau}_{out}$ can be represented as

$$\hat{\boldsymbol{\tau}}_{out} = \boldsymbol{z} + \boldsymbol{p}(\boldsymbol{q}_e, \dot{\boldsymbol{q}}_e). \tag{16}$$

The process of the design and analysis of the contact force estimator has been presented above. To ensure that the appropriate $X$ is obtained, the convergence of the tracking error of the contact force estimator should be further analysed.

### 3.2. Stability of the contact force estimator

As shown in the previous subsection, the contact force between the foot of the quadruped robot and the ground can be estimated by means of (9). Suppose that the quadruped robot is moving on homogeneous ground and that the external contact force between the foot end and the ground remains basically unchanged, that is, $\dot{\boldsymbol{\tau}}_{out} \approx 0$; then, the following theorem can guarantee the asymptotic stability of the foot-end force estimation error for the quadruped robot.

**Theorem 1:** For a quadruped robot, the contact force can be estimated by means of (9). If $X$ satisfies the following conditions, then the contact force tracking error $\widetilde{\boldsymbol{\tau}}_{out} = \boldsymbol{\tau}_{out} - \hat{\boldsymbol{\tau}}_{out}$ will converge to zero

1) The matrix $X$ is invertible.
2) There exists a positive definite and symmetric matrix $\chi$ satisfying $X + X^T - X^T\dot{\boldsymbol{M}}_e X \geq \chi$.

**Proof:** The following energy function is considered

$$\begin{aligned} W &= (X\widetilde{\boldsymbol{\tau}}_{out})^{\mathrm{T}}\boldsymbol{M}_e(X\widetilde{\boldsymbol{\tau}}_{out}) \\ &= \widetilde{\boldsymbol{\tau}}_{out}^{\mathrm{T}}X^{\mathrm{T}}\boldsymbol{M}_e X\widetilde{\boldsymbol{\tau}}_{out}. \end{aligned} \tag{17}$$

Since $\boldsymbol{M}_e$ is a symmetric and positive matrix, $X$ is invertible, and $X^{\mathrm{T}}M_eX$ is positive definite, the energy function $W$ is also positive definite and $W \to \infty$.

When $\dot{\boldsymbol{\tau}}_{out} \approx 0$, the derivative of (17) can be calculated to obtain

$$\begin{aligned} \dot{W} = {} & \dot{\widetilde{\boldsymbol{\tau}}}_{out}^{\mathrm{T}}X^{\mathrm{T}}\boldsymbol{M}_e\mathbf{X}\widetilde{\boldsymbol{\tau}}_{out} + \widetilde{\boldsymbol{\tau}}_{out}^{\mathrm{T}}\mathbf{X}^{\mathrm{T}}\boldsymbol{M}_e\mathbf{X}\dot{\widetilde{\boldsymbol{\tau}}}_{out} \\ & + \widetilde{\boldsymbol{\tau}}_{out}^{\mathrm{T}}X^{\mathrm{T}}\dot{\boldsymbol{M}}_e X\widetilde{\boldsymbol{\tau}}_{out}. \end{aligned} \tag{18}$$

Because $\widetilde{\boldsymbol{\tau}}_{out} = \boldsymbol{\tau}_{out} - \hat{\boldsymbol{\tau}}_{out}$, it holds that

$$\dot{\widetilde{\boldsymbol{\tau}}}_{out} = \dot{\boldsymbol{\tau}}_{out} - \dot{\hat{\boldsymbol{\tau}}}_{out}. \tag{19}$$

Substituting (10) into (19) results in

$$\dot{\widetilde{\boldsymbol{\tau}}}_{out} = \dot{\boldsymbol{\tau}}_{out} - \boldsymbol{L}(\boldsymbol{q}_e, \dot{\boldsymbol{q}}_e)\widetilde{\boldsymbol{\tau}}_{out}. \tag{20}$$

Substituting (12) and (20) into (18) yields

$$\dot{W} = -\widetilde{\boldsymbol{\tau}}_{out}^{\mathrm{T}}(X + X^{\mathrm{T}} - X^{\mathrm{T}}\dot{\boldsymbol{M}}_e X)\widetilde{\boldsymbol{\tau}}_{out}. \tag{21}$$

According to the energy functions $W > 0$, $X + X^T - X^T\dot{\boldsymbol{M}}_e X \geq \chi$, and $\dot{W} < 0$, it can be concluded that the contact force tracking error asymptotically converges to zero. This completes the proof. □

## 4. DESIGN OF THE VARIABLE IMPEDANCE CONTROLLER

The essence of impedance control is based on the virtual concept of "mechanical impedance" and the principle of feedback equivalence. One of the most important advantages of impedance control is that the force control target and displacement control target are unified in the target system to dynamically adjust the motion and contact force of the end effector. In invariant impedance control, the force and position constraints in the control task target are constant constraints, so the control problem is a problem of fixed-point adjustment. However, in variable impedance control, the control target is a "time-varying impedance contour or trajectory". For complex systems such as assembly robots, grinding robots, and exoskeleton robots, the inertia, damping and stiffness parameters are varying in time during the execution of the operation tasks, so constant impedance control cannot guarantee the performance of such a system.

To improve the dynamic performance of the foot of a quadruped robot in contact with the ground and adjust the interaction state between the quadruped robot and its environment in real time, the dynamics model of the closed-loop system for variable impedance control is established as follows [37]:

$$\boldsymbol{H}(t)\ddot{\bar{\boldsymbol{q}}}_e + \boldsymbol{D}(t)\dot{\bar{\boldsymbol{q}}}_e + \boldsymbol{K}(t)\bar{\boldsymbol{q}}_e = \boldsymbol{\tau}_{out}, \tag{22}$$

where $\boldsymbol{H}(t)$, $\boldsymbol{D}(t)$, and $\boldsymbol{K}(t)$ are symmetric positive time-varying matrices. $\boldsymbol{H}(t)$ represents the desired inertia matrix, $\boldsymbol{D}(t)$ denotes the desired damping matrix, and $\boldsymbol{K}(t)$ is the desired stiffness matrix. It is supposed that $\ddot{\bar{\boldsymbol{q}}}_e = \ddot{\boldsymbol{q}}_e - \ddot{\boldsymbol{q}}_{ed}$, $\dot{\bar{\boldsymbol{q}}}_e = \dot{\boldsymbol{q}}_e - \dot{\boldsymbol{q}}_{ed}$, and $\bar{\boldsymbol{q}}_e = \boldsymbol{q}_e - \boldsymbol{q}_{ed}$ are the errors in acceleration, velocity and position, respectively, where $\ddot{\boldsymbol{q}}_{ed} = \begin{bmatrix}\ddot{x}_d & \ddot{y}_d & \ddot{z}_d\end{bmatrix}^{\mathrm{T}}$, $\dot{\boldsymbol{q}}_{ed} = \begin{bmatrix}\dot{x}_d & \dot{y}_d & \dot{z}_d\end{bmatrix}^{\mathrm{T}}$, and $\boldsymbol{q}_{ed} = \begin{bmatrix}x_d & y_d & z_d\end{bmatrix}^{\mathrm{T}}$ are the desired acceleration, desired speed and desired position of the foot, respectively, associated with the desired gait.

By combining the single-leg dynamics model (8) of the quadruped robot with the variable impedance control dynamics model (22), the control law for variable impedance control can be derived as follows:

$$\begin{cases} \boldsymbol{\tau}_e = \boldsymbol{M}_e\boldsymbol{v} + \boldsymbol{C}_e\dot{\boldsymbol{q}}_e + \boldsymbol{G}_e - \boldsymbol{\tau}_{out}, \\ \boldsymbol{v} = \ddot{\boldsymbol{q}}_{ed} + (\boldsymbol{H}(t))^{-1}(\boldsymbol{\tau}_e - \boldsymbol{K}(t)\bar{\boldsymbol{q}}_e - \boldsymbol{D}(t)\dot{\bar{q}}_e). \end{cases} \tag{23}$$

To ensure the stability of the closed-loop system, in accordance with Lyapunov stability theory, the following energy function is selected [38]

$$\begin{aligned} \mathbf{V} = {} & \frac{1}{2}(\dot{\bar{\boldsymbol{q}}}_e + \alpha\bar{\boldsymbol{q}}_e)^{\mathrm{T}}\boldsymbol{H}(t)(\dot{\bar{\boldsymbol{q}}}_e + \alpha\bar{\boldsymbol{q}}_e) \\ & + \frac{1}{2}\bar{\boldsymbol{q}}_e^{\mathrm{T}}\beta(t)\bar{\boldsymbol{q}}_e, \end{aligned} \tag{24}$$

where $\alpha$ is a constant satisfying $\alpha > 0$ and $\beta(t)$ is an undetermined time-varying matrix satisfying $\beta(t) > 0$. The above conditions $\alpha > 0$ and $\beta(t) > 0$ ensure the positive definiteness of the Lyapunov function $V$.

**Assumption 1:** The inertia $\boldsymbol{H}(t)$, damping $\boldsymbol{D}(t)$, and stiffness $\boldsymbol{K}(t)$ are set to be symmetric, uniformly continuous functions, and $\boldsymbol{H}(t) > 0$, $\boldsymbol{D}(t) > 0$, and $\boldsymbol{K}(t) > 0$. In other words, the time derivatives $\dot{\boldsymbol{H}}(t)$, $\dot{\boldsymbol{D}}(t)$, and $\dot{\boldsymbol{K}}(t)$ are bounded for all $t > 0$.

**Assumption 2:** There always exists a matrix $\boldsymbol{D}_0(t)$ such that $\dot{\boldsymbol{H}}(t) - 2\boldsymbol{D}_0(t)$ is skew symmetric.

The inertia $\boldsymbol{H}(t)$ determines the stability of the system, and too large or too small of a value will affect the system performance.

**Assumption 3:** Conservative constraints on $\boldsymbol{H}(t)$ are given by $\boldsymbol{M}_e$, and $\boldsymbol{H}(t)$ is chosen such that

$$\lambda_{\min}(\boldsymbol{M}_e)\mathrm{I} \leq \boldsymbol{H}(t) \leq \lambda_{\max}(\boldsymbol{M}_e)\mathrm{I}.$$

**Theorem 2:** Suppose that Assumptions 1-3 hold. Considering the single-leg dynamics model (8) of the quadruped robot and the target variable impedance control dynamics model (22), suppose that the following set of inequalities holds

$$\begin{cases} \alpha > 0, \\ \boldsymbol{K}(t) + \alpha \boldsymbol{D}(t) - \alpha^2 \boldsymbol{H}(t) - 2\alpha \boldsymbol{D}_0(t) > 0, \\ \boldsymbol{D}(t) - \alpha \boldsymbol{H}(t) - \boldsymbol{D}_0(t) > 0, \\ \alpha \dot{\boldsymbol{K}}(t) - \frac{1}{2}\dot{\boldsymbol{K}}(t) - \frac{1}{2}\alpha \dot{\boldsymbol{D}}(t) + \alpha \dot{\boldsymbol{D}}_0(t) > 0. \end{cases} \tag{25}$$

When $\boldsymbol{\tau}_{out} = 0$, the origin $\bar{\boldsymbol{q}}_e = 0$ of the variable impedance control dynamics model (22) is globally asymptotically stable. When $\boldsymbol{\tau}_{out} \neq 0$, the origin $\bar{\boldsymbol{q}}_e = 0$ of the system described by (22) is globally stable under the same conditions.

**Proof:** The time derivative of the Lyapunov energy function can be calculated as follows:

$$\begin{aligned} \dot{\mathbf{V}} = {} & (\dot{\bar{\boldsymbol{q}}}_e + \alpha \bar{\boldsymbol{q}}_e)^{\mathrm{T}} \boldsymbol{H}(t)(\ddot{\bar{\boldsymbol{q}}}_e + \alpha \dot{\bar{\boldsymbol{q}}}_e) \\ & + \frac{1}{2}(\dot{\bar{\boldsymbol{q}}}_e + \alpha \bar{\boldsymbol{q}}_e)^{\mathrm{T}} \dot{\boldsymbol{H}}(t)(\dot{\bar{\boldsymbol{q}}}_e + \alpha \bar{\boldsymbol{q}}_e) \\ & + \dot{\bar{\boldsymbol{q}}}_e^{\mathrm{T}} \beta(t) \bar{\boldsymbol{q}}_e + \frac{1}{2}\bar{q}_e^{\mathrm{T}} \dot{\beta}(t) \bar{\boldsymbol{q}}_e. \end{aligned} \tag{26}$$

Upon substituting the resulting dynamics function $\boldsymbol{H}(t)\ddot{\bar{\boldsymbol{q}}}_e = \boldsymbol{\tau}_{out} - \boldsymbol{K}(t)\bar{\boldsymbol{q}}_e - \boldsymbol{D}(t)\dot{\bar{\boldsymbol{q}}}_e$ into (26), it follows that

$$\begin{aligned} \dot{\mathbf{V}} = {} & (\dot{\bar{\boldsymbol{q}}}_e + \alpha \bar{\boldsymbol{q}}_e)^{\mathrm{T}} \boldsymbol{\tau}_{out} - \dot{\bar{\boldsymbol{q}}}_e^{\mathrm{T}} (\boldsymbol{D}(t) \\ & - \alpha \boldsymbol{H}(t) - \frac{1}{2}\dot{\boldsymbol{H}}(t)) \dot{\bar{\boldsymbol{q}}}_e - \dot{\bar{\boldsymbol{q}}}_e^{\mathrm{T}} (\boldsymbol{K}(t) \\ & + \alpha \boldsymbol{D}(t) - \alpha^2 \boldsymbol{H}(t) - \alpha \dot{\boldsymbol{H}}(t) \\ & - \beta(t)) \bar{\boldsymbol{q}}_e - \bar{\boldsymbol{q}}_e^{\mathrm{T}} (\alpha \boldsymbol{K}(t) \\ & - \frac{1}{2}\alpha^2 \dot{H}(t) - \frac{1}{2}\dot{\beta}(t)) \bar{\boldsymbol{q}}_e. \end{aligned} \tag{27}$$

By eliminating the nonquadratic term in (26), the positive definiteness of the Lyapunov function is automatically guaranteed. By setting $\beta(t) = \boldsymbol{K}(t) + \alpha \boldsymbol{D}(t) - \alpha^2 \boldsymbol{H}(t) - \alpha \dot{\boldsymbol{H}}(t) > 0$ and taking the derivative of $\beta(t)$, one obtains

$$\dot{\beta}(t) = \dot{\boldsymbol{K}}(t) + \alpha \dot{\boldsymbol{D}}(t) - \alpha^2 \dot{\boldsymbol{H}}(t) - \alpha \ddot{\boldsymbol{H}}(t) > 0. \tag{28}$$

By substituting (28) into (27), (27) can be written in a more concise form

$$\begin{aligned} \dot{\mathbf{V}} = {} & (\dot{\bar{\boldsymbol{q}}}_e + \alpha \bar{\boldsymbol{q}}_e)^{\mathrm{T}} \boldsymbol{\tau}_{out} - \dot{\bar{\boldsymbol{q}}}_e^{\mathrm{T}} (\boldsymbol{D}(t) - \alpha \boldsymbol{H}(t) \\ & - \frac{1}{2}\dot{\boldsymbol{H}}(t)) \dot{\bar{\boldsymbol{q}}}_e - \bar{\boldsymbol{q}}_e^{\mathrm{T}} (\alpha \dot{\boldsymbol{K}}(t) - \frac{1}{2}\dot{\boldsymbol{K}}(t) \\ & - \frac{1}{2}\alpha \dot{\boldsymbol{D}}(t) + \frac{1}{2}\alpha \ddot{\boldsymbol{H}}(t)) \bar{\boldsymbol{q}}_e. \end{aligned} \tag{29}$$

For a given $\boldsymbol{H}(t)$, there always exists a $\boldsymbol{D}_0(t)$ such that $\dot{\boldsymbol{H}}(t) - 2\boldsymbol{D}_0(t)$ is skew symmetric, i.e., $(\dot{\bar{\boldsymbol{q}}}_e + \alpha \bar{\boldsymbol{q}}_e)^{\mathrm{T}} (\dot{\boldsymbol{H}}(t) - 2\boldsymbol{D}_0(t))(\ddot{\bar{\boldsymbol{q}}}_e + \alpha \dot{\bar{\boldsymbol{q}}}_e) = 0$. Substituting $\boldsymbol{D}_0(t)$ for $\dot{\boldsymbol{H}}(t)$ in (29) leads to

$$\begin{aligned} \dot{\mathbf{V}} = {} & (\dot{\bar{\boldsymbol{q}}}_e + \alpha \bar{\boldsymbol{q}}_e)^{\mathrm{T}} \tau_{out} - \dot{\bar{\boldsymbol{q}}}_e^{\mathrm{T}} (\boldsymbol{D}(t) \\ & - \alpha \boldsymbol{H}(t) - \boldsymbol{D}_0(t)) \dot{\bar{\boldsymbol{q}}}_e - \bar{\boldsymbol{q}}_e^{\mathrm{T}} (\alpha \dot{\boldsymbol{K}}(t) \\ & - \frac{1}{2}\dot{\boldsymbol{K}}(t) - \frac{1}{2}\alpha \dot{\boldsymbol{D}}(t) + \alpha \dot{\boldsymbol{D}}_0(t)) \bar{\boldsymbol{q}}_e. \end{aligned} \tag{30}$$

Next, the stability of the closed-loop system in the noncontact phase and in the contact phase, i.e., when $\boldsymbol{\tau}_{out} = 0$ and $\boldsymbol{\tau}_{out} \neq 0$, will be discussed.

1) When the contact forces satisfy $\boldsymbol{\tau}_{out} = 0$, then (30) will result in

$$\begin{aligned} \dot{\mathbf{V}} = {} & -\dot{\bar{\boldsymbol{q}}}_e^{\mathrm{T}} (\boldsymbol{D}(t) - \alpha \boldsymbol{H}(t) \\ & - \boldsymbol{D}_0(t)) \dot{\bar{\boldsymbol{q}}}_e - \bar{\boldsymbol{q}}_e^{\mathrm{T}} (\alpha \dot{\boldsymbol{K}}(t) \\ & - \frac{1}{2}\dot{\boldsymbol{K}}(t) - \frac{1}{2}\alpha \dot{\boldsymbol{D}}(t) + \alpha \dot{\boldsymbol{D}}_0(t)) \bar{\boldsymbol{q}}_e. \end{aligned} \tag{31}$$

To ensure that $\dot{V} < 0$, the following set of inequalities must be satisfied

$$\begin{cases} \boldsymbol{D}(t) - \alpha \boldsymbol{H}(t) - \frac{1}{2}\dot{\boldsymbol{H}}(t) > 0, \\ \alpha \dot{\boldsymbol{K}}(t) - \frac{1}{2}\dot{\boldsymbol{K}}(t) - \frac{1}{2}\alpha \dot{\boldsymbol{D}}(t) + \frac{1}{2}\alpha \dot{\boldsymbol{D}}_0(t) > 0. \end{cases} \tag{32}$$

The energy function $V$ is positive definite and $\dot{V}$ is negative definite, then when $\bar{\boldsymbol{q}}_e \to \infty$, $\dot{\bar{\boldsymbol{q}}}_e \to \infty$, $V \to \infty$ is unbounded. When $t \to \infty$, $\bar{\boldsymbol{q}}_e \to 0$, $\dot{\bar{\boldsymbol{q}}}_e \to 0$, the closed-loop system is globally asymptotically stable. Thus, the closed-loop system (23) is stable in the noncontact phase.

2) When the contact forces satisfy $\boldsymbol{\tau}_{out} \neq 0$, if the inequalities in (32) still hold, then

$$\dot{\mathbf{V}} \leq \left(\dot{\bar{\boldsymbol{q}}}_e + \alpha \bar{\boldsymbol{q}}_e\right)^{\mathrm{T}} \boldsymbol{\tau}_{out}. \tag{33}$$

Then,

$$\mathbf{V} \leq \mathbf{V}(0) + \int_0^t (\dot{\bar{\boldsymbol{q}}}_e + \alpha \bar{\boldsymbol{q}}_e)^{\mathrm{T}} \boldsymbol{\tau}_{out} d\rho. \tag{34}$$

The above inequality (34) is called the dissipation function [31]. Dissipation ensures stable behaviour of the system in the contact phase.

Based on the above analysis, the following must hold

$$\begin{cases} \alpha > 0, \\ \boldsymbol{K}(t) + \alpha \boldsymbol{D}(t) - \alpha^2 \boldsymbol{H}(t) - 2\alpha \boldsymbol{D}_0(t) > 0, \\ \boldsymbol{D}(t) - \alpha \boldsymbol{H}(t) - \boldsymbol{D}_0(t) > 0, \\ \alpha \dot{\boldsymbol{K}}(t) - \frac{1}{2}\dot{\boldsymbol{K}}(t) - \frac{1}{2}\alpha \dot{\boldsymbol{D}}(t) + \alpha \dot{\boldsymbol{D}}_0(t) > 0. \end{cases} \tag{35}$$

The closed-loop system (23) is stable. This completes the proof. □

**Remark 1:** The inequalities $\alpha > 0$ and $\beta(t) = \boldsymbol{K}(t) + \alpha \boldsymbol{D}(t) - \alpha^2 \boldsymbol{H}(t) - \alpha \dot{\boldsymbol{H}}(t) > 0$ guarantee the positive definiteness of the Lyapunov energy function. To better adapt to changes in the environment, the update law for the stiffness matrix $\boldsymbol{K}(t)$ should be selected in accordance with the specific terrain.

**Remark 2:** In this paper, the variable impedance control performance in the stance phase and the swing phase is analysed; however, a more suitable controller for the swing phase still needs to be designed.

## 5. NUMERICAL SIMULATION

To verify the effectiveness of the proposed variable impedance control scheme for a single leg of a quadruped robot in the stance phase, a simulation model was built in MATLAB. The simulation model is shown in Fig. 3.

As shown in Fig. 3, the simulation model is mainly composed of five parts: the desired gait, the control law, the controlled plant, the force estimator, and the output module. In Fig. 3, the desired gait is described by (36) below. With the desired gait, the kinematics and dynamics models and the proposed variable impedance control scheme, the control law for the closed-loop system can be expressed as shown in (23). Through the control law module, the control torque is obtained and transmitted to the controlled plant (7); then, the actual position and attitude of the system can be acquired. The foot follows a simple cycloid trajectory, as follows:

$$\begin{cases} x = (x_f - x_s)\frac{\sigma - \sin\sigma}{2\pi} + x_s, \\ z = h\frac{1-\cos\sigma}{2} + z_s, \end{cases} \qquad \sigma = \frac{2\pi t}{T_s}. \tag{36}$$

In this paper, only $x$ and $z$ are planned; the trajectory parameters, the structural parameters of the single leg and the variable impedance control parameters are given in Table 1.

The closed-loop system (23) was simulated in MATLAB. Under the assumption that the contact forces are $\boldsymbol{\tau}_{out} = [0,0,0]^{\mathrm{T}}$, the position response curve, position error curve, actuation torque response curve and contact force estimation curve in a single cycle are illustrated in Figs. 4-7.

It can be seen from Figs. 4 and 5 that when the contact forces are $\boldsymbol{\tau}_{out} = [0,\ 0,\ 0]^{\mathrm{T}}$, the quadruped robot starts from -0.1 m to 0.1 m in $x$ and lifts its leg up 0.15 m in $z$ at $-0.482$ m. When the variable impedance control scheme is used, the quadruped robot can track the desired trajectory well. In this paper, since only $x$ and $z$ of the foot are planned, $y$ is always maintained at $-0.15$ m. Moreover, 0

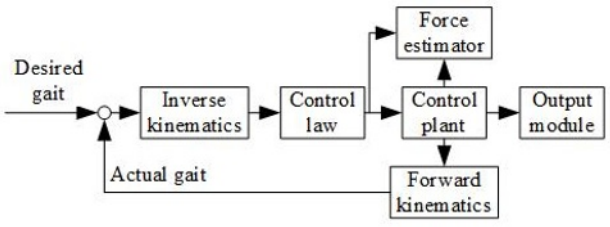


Fig. 3. Simulation model of variable impedance control.

Table 1. Trajectory parameters, structural parameters, and variable impedance control parameters.

| Parameter | Symbol | Value |
|---|---|---|
| Period | $T$ | 1 s |
| Swing period | $T_s$ | 0.25 s |
| Starting point | $x_s$ | $-0.1$ m |
| Terminal point | $x_f$ | 0.1 m |
| Initial height | $z_s$ | $-0.482$ m |
| Leg lift height | $h$ | 0.15 m |
| Hip length | $l_1$ | 0.15 m |
| Thigh length | $l_2$ | 0.35 m |
| Calf length | $l_3$ | 0.382 m |
| Hip mass | $m_1$ | 0.1 kg |
| Thigh mass | $m_2$ | 0.3 kg |
| Calf mass | $m_3$ | 0.4 kg |
| Variable inertia matrix | $\boldsymbol{H}(t)$ | $diag(0.00025 + 0.0001 * \sin(\frac{\pi}{2} * t))$ |
| Variable damping matrix | $\boldsymbol{D}(t)$ | $diag(0.05 + 0.01 * \sin(\frac{\pi}{2} * t))$ |
| Variable stiffness matrix | $\boldsymbol{K}(t)$ | $diag(4 + 0.01 * \sin(\frac{\pi}{2} * t))$ |
| Constant | $\alpha$ | 2 |

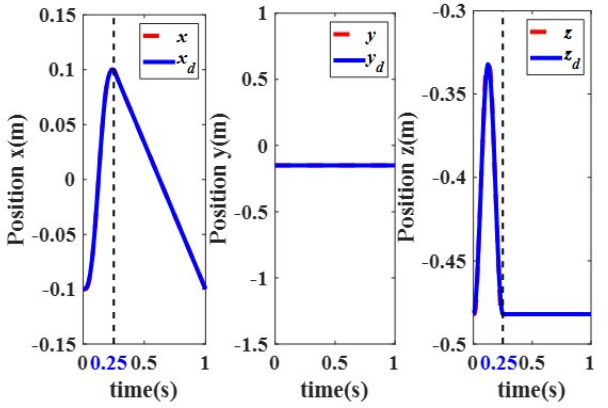


Fig. 4. Position response curve under variable impedance control.

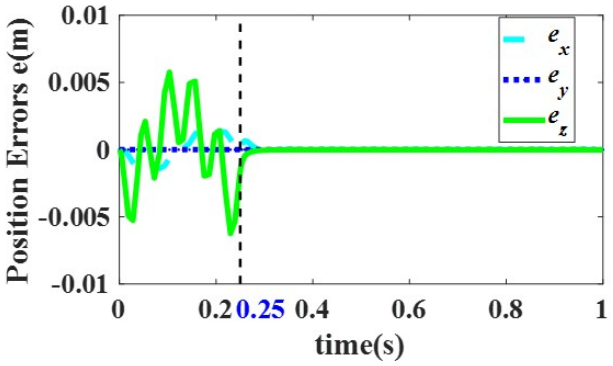


Fig. 5. Position error response curve under variable impedance control.

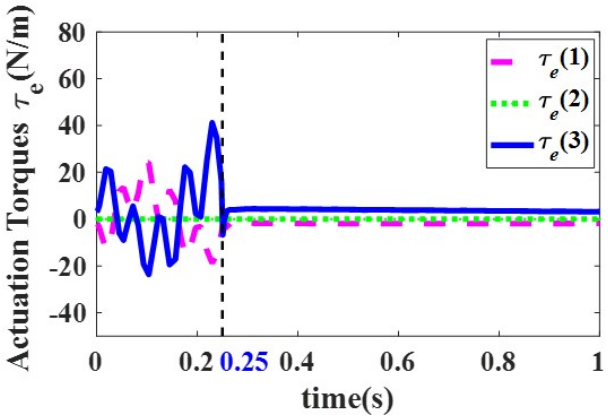


Fig. 6. Actuation torque response curve under variable impedance control.

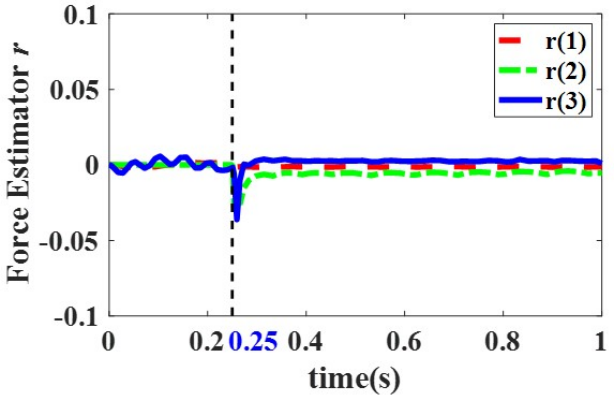


Fig. 7. Force estimation curve under variable impedance control.

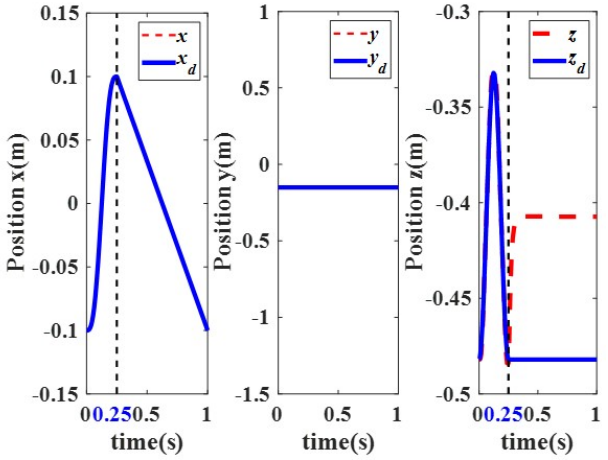


Fig. 8. Position response curve under variable impedance control.

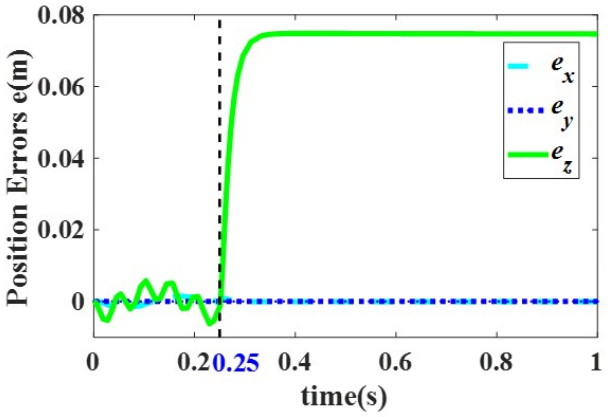


Fig. 9. Position error response curve under variable impedance control.

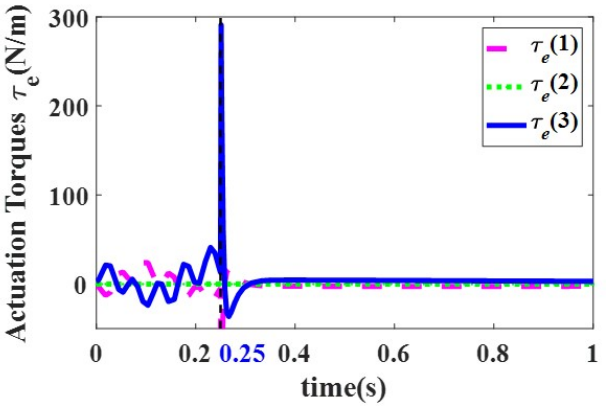


Fig. 10. Actuation torque response curve under variable impedance control.

0.25 s is the swing period, and 0.25-1 s is the stance phase. The controller presented in this paper is mainly designed for the stance phase. In the future, it will be necessary to further adjust the variable impedance control parameters or improve the design of the controller to overcome the problems of the large swing period error and driving torque fluctuations observed in Figs. 5 and 6. Fig. 7 shows the force estimation curve, from which it is obvious that the force estimator designed in this paper can successfully estimate the foot forces.

For contact forces of $\boldsymbol{\tau}_{out} = \left[0,\ 0,\ 0.3\right]^{\mathrm{T}}$ in the stance phase, the closed-loop system (23) was further simulated to obtain the corresponding position response curve, position error curve, driving torque response curve and force estimation curve in a single period, which are shown in Figs. 8-11.

The simulation results in Figs. 4-7 and Figs. 8-11 show that the foot end of the quadruped robot can track the desired trajectory and that the position tracking error converges to 0. The variable impedance control of the closed-loop system is stable. In contrast to Fig. 4, the contact force in Fig. 8 is not zero in the stance phase, and the variable impedance controller has to adjust the foot position to ensure that the foot contact force is stable at the desired value. As seen by comparing Fig. 6 and Fig. 10, due to the different external forces, the value of the actuation torque

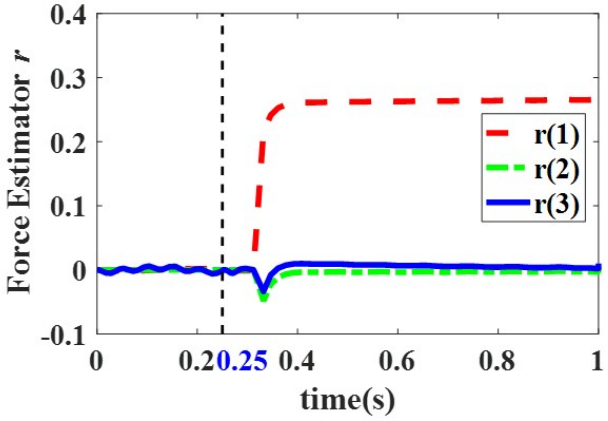


Fig. 11. Force estimation curve under variable impedance control.

will change accordingly. The simulation results in Figs. 7 and 11 further illustrate that the proposed force estimator based on a nonlinear disturbance observer is feasible. Taken together, Figs. 4-7 and Figs. 8-11 show that the theoretical analysis is consistent with the simulation results.

## 6. CONCLUSION

Currently, quadruped robots are attracting increasing attention in patrol, rescue and home service applications due to various advantages, such as their adaptability to rough terrain. One important issue in the field of quadruped robots is the stability of their motion, especially when such a robot interacts with its environment, resulting in impact. Impedance control can stabilize the desired motion and the interaction forces during a given operation task. In this paper, variable impedance control based on the operation space is studied to ensure the stability of the system. However, the time-varying impedance control parameters continuously inject potential energy into the system, making traditional stability analysis methods no longer applicable. Instead, the stability of variable impedance control in the operation space is analysed by applying a new Lyapunov function. Moreover, by designing a force estimator acting in the operation space, the installation of force sensors is avoided. The design process and the convergence of the contact force tracking error are analysed in detail. The feasibility of the proposed variable impedance controller and the nonlinear contact force estimator acting in the operation space is demonstrated through numerical simulations.

## CONFLICT OF INTEREST

The authors declare that there is no competing financial interest or personal relationship that could have appeared to influence the work reported in this paper.

## REFERENCES

[1] Y. Farid, V. J. Majd, and A. Ehsani-Seresht, "Dynamic-free robust adaptive intelligent fault-tolerant controller design with prescribed performance for stable motion of quadruped robots," *Adaptive Behavior*, vol. 29, no. 3, pp. 233-252, 2021.

[2] Y. Tan, Z. Chao, and S. Han, "Trotting control of load-carrying quadruped walking vehicle with load variations based on the centroidal dynamics and adaptive sliding mode control," *Mathematical Problems in Engineering*, vol. 2020, Article ID 7154254, 2020.

[3] L. Wang, L. Meng, and R. Kang, "Design and dynamic locomotion control of quadruped robot with perception-less terrain adaptation," *Cyborg and Bionic Systems*, vol. 2022, ArticleID 9816495, 2022.

[4] N. Hu, S. Li, and F. Gao, "Multi-objective hierarchical optimal control for quadruped rescue robot," *International Journal of Control, Automation, and Systems*, vol. 16, no. 4, pp. 1866-1877, 2018.

[5] S. Seok, A. Wang, and M. Y. Chuah, "Design principles for energy-efficient legged locomotion and implementation on the MIT Cheetah robot," *IEEE/ASME Transactions on Mechatronics*, vol. 20, no. 3, pp. 1117-1129, 2014.

[6] R. Zhu, Q. Yang, and Y. Liu, "Sliding mode robust control of hydraulic drive unit of hydraulic quadruped robot," *International Journal of Control, Automation, and Systems*, vol. 20, no. 4, pp. 1336-1350, 2022.

[7] V. G. Loc, S. Roh, and I. M. Koo, "Sensing and gait planning of quadruped walking and climbing robot for traversing in complex environment," *Robotics and Autonomous Systems*, vol. 58, no. 5, pp. 666-675, 2010.

[8] M. Hutter, C. Gehring, and D. Jud, "Anymal-a highly mobile and dynamic quadrupedal robot," *Proc. of IEEE/RSJ International Conference on Intelligent Robots and Systems (IROS)*, pp. 38-44, 2016.

[9] M. Li, Z. Jiang, and P. Wang, "Control of a quadruped robot with bionic springy legs in trotting gait," *Journal of Bionic Engineering*, vol. 11, no. 1, pp. 188-198, 2014.

[10] M. H. Raibert, and J. J. Craig, "Hybrid position/force control of manipulators," *Journal of Dynamic Systems, Measurement, and Control*, vol. 103, no. 2, pp. 188-198, 2014.

[11] N. Hogan, "Impedance control: An approach to manipulation: Part I-Theory," *Dynamic Systems, Measurement and Control*, vol. 107, no. 1, pp. 1-7, 1985.

[12] S. Yi, "Stable walking of quadruped robot by impedance control for body motion," *International Journal of Control and Automation*, vol. 6, no. 2, pp. 99-110, 2013.

[13] L. Xiao, T. Yang, and B. Huo, "Impedance control of a robot needle with a fiber optic force sensor," *Proc. of IEEE 13th International Conference on Signal Processing (ICSP)*, pp. 1379-1383, 2016.

[14] E. Akdoğan, M. E. Aktan, and A. T. Koru, "Hybrid impedance control of a robot manipulator for wrist and forearm rehabilitation: Performance analysis and clinical results," *Mechatronics*, vol. 49, pp. 77-91, 2018.

[15] W. Huo, S. Mohammed, and Y. Amirat, "Active impedance control of a lower limb exoskeleton to assist sit-to-stand movement," *Proc. of IEEE International Conference on Robotics and Automation (ICRA)*, pp. 3530-3536, 2016.

[16] H. Ochoa and R. Cortesao, "Impedance control architecture for robotic-assisted mold polishing based on human demonstration," *IEEE Transactions on Industrial Electronics*, pp. 1-9, 2021.

[17] K. Lee and M. Buss, "Force tracking impedance control with variable target stiffness," *Proc. of the 17th World Congress*, vol. 41, no. 2, pp. 6751-6756, 2008.

[18] M. Bednarczyk, H. Omran, and B. Bayle, "Passivity filter for variable impedance control," *Proc. of IEEE/RSJ International Conference on Intelligent Robots and Systems (IROS)*, pp. 7159-7164, 2020.

[19] J. Wei, D. Yi, and X. Bo, "Adaptive variable parameter impedance control for apple harvesting robot compliant picking," *Complexity*, pp. 1-15, 2020.

[20] K. Ba, G. Ma, and B. Yu, "A nonlinear model-based variable impedance parameters control for position-based impedance control system of hydraulic drive unit," *International Journal of Control, Automation, and Systems*, vol. 18, no. 7, pp. 1806-1817, 2020.

[21] F. Ferraguti, C. Secchi, and C. Fantuzzi, "A tank-based approach to impedance control with variable stiffness," *Proc. of IEEE International Conference on Robotics and Automation*, pp. 4948-4953, 2013.

[22] A. Dietrich, X. Wu, and K. Bussmann, "Passive hierarchical impedance control via energy tanks," *IEEE Robotics and Automation Letters*, vol. 2, no. 2, pp. 522-529, 2016.

[23] J. Park and Y. Choi, "Input-to-state stability of variable impedance control for robotic manipulator," *Applied Sciences*, vol. 12, no. 4, pp. 522-529, 2016.

[24] K. Kronander and A. Billard, "Stability considerations for variable impedance control," *IEEE Transactions on Robotics*, vol. 32, no. 5, pp. 1298-1305, 2016.

[25] L. P. J. Selen, D. W. Franklin, and D. M. Wolpert, "Impedance control reduces instability that arises from motor noise," *Journal of Neuroscience*, vol. 29, no. 40, pp. 12606-12616, 2009.

[26] K. Ba, B. Yu, and Z. Gao, "Parameters sensitivity analysis of position-based impedance control for bionic legged robots' HDU," *Applied Sciences*, vol. 7, no. 10, pp. 1-20, 2017.

[27] G. Peng, C. Yang, W. He, and C. L. P. Chen, "Force sensorless admittance control with neural learning for robots with actuator saturation," *IEEE Transactions on Industrial Electronics*, vol. 67, no. 40, pp. 1-10, 2019.

[28] A. Mohammadi, M. Tavakoli, and H. J. Marquez, "Nonlinear disturbance observer design for robotic manipulators," *Control Engineering Practice*, vol. 21, no. 3, pp. 253-267, 2013.

[29] R. M. Murray, Z. Li, and S. S. Sastry, *A Mathematical Introduction Torobotic Manipulation*, CRC press, Boca Raton, 1994.

[30] A. B. Tatar, B. Taşar, and O. Yakut, "A shooting and control application of four-legged robots with a gun turret," *Arabian Journal for Science and Engineering*, vol. 45, no. 7, pp. 5191-5206, 2020.

[31] Y. T. Dong and B. B. Ren, "UDE-based variable impedance control of uncertain robot systems," *IEEE Transactions on Systems, Man, and Cybernetics: Systems*, vol. 49, no. 12, pp. 1-12, 2017.

[32] D. Luca, A. Albu-Schaffer, and S. Haddadin, "Collision detection and safe reaction with the DLR-III lightweight manipulator arm," *Proc. of IEEE/RSJ International Conference on Intelligent Robots and Systems*, pp. 1623-1630, 2006.

[33] P. J. Hacksel, and S. E. Salcudean, "Estimation of environment forces and rigid-body velocities using observers," *Proc. of the 1994 IEEE International Conference on Robotics and Automation*, pp. 1623-1630, 1994.

[34] K. S. Eom, I. H. Suh, and W. K. Chung, "Disturbance observer based path tracking control of robot manipulator considering torque saturation," *Proc. of 1997 8th International Conference on Advanced Robotics*, pp. 651-657, 1997.

[35] N. Dini and V. J. Majd, "Sliding-Mode tracking control of a walking quadruped robot with a push recovery algorithm using a nonlinear disturbance observer as a virtual force sensor," *Iranian Journal of Science and Technology, Transactions of Electrical Engineering*, vol. 44, no. 3, pp. 1033-1057, 2020.

[36] A. Shiva, A. Stilli, and Y. Noh, "Tendon-based stiffening for a pneumatically actuated soft manipulator," *IEEE Robotics and Automation Letters*, vol. 1, no. 2, pp. 632-637, 2016.

[37] G. P. He, Y. N. Fan, and T. T. Su, "Variable impedance control of cable actuated continuum manipulators" *International Journal of Control, Automation, and Systems*, vol. 18, no. 7, pp. 1839-1852, 2020.

[38] T. T. Su, L. Z. Niu, G. P. He, X. Liang, L. Zhao, and Q. Zhao, "Coordinated variable impedance control for multi-segment cable-driven continuum manipulators," *Mechanism and Machine Theory*, vol. 153, 103969, 2020.

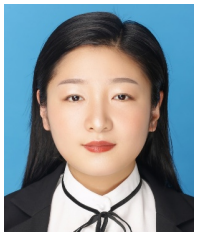

**Yanan Fan** received her M.S. degree from the Department of Mechanical and Materials Engineering, North China University of Technology, Beijing, China. Currently she is a doctor in the School of Automation Science and Electrical Engineering, Beihang University, Beijing 100191, China. Her research interests in dynamics and control of robot.

**Zhongcai Pei** received his B.S., M.S., and Ph.D. degrees in mechanical and electrical engineering from Harbin Institute of Technology University of China, Haerbin, China, in 1991, 1994, and 1997, respectively. He is currently with the School of Automation Science and Electrical Engineering, Beihang University, Beijing, China. His current research interests include robot technology and electro-hydraulic servo control.

**Zhiyong Tang** received his B.S. degree in fluid power transmission and control from Beihang University in 1997 and his Ph.D. degree in mechanical and electrical engineering from Beihang University in 2003. He is currently with the School of Automation Science and Electrical Engineering, Beihang University, Beijing, China. His research interests include electro-hydraulic servo control and intelligent robot system.